Materials & Design 229 (2023) 111908

Contents lists available at ScienceDirect

Materials & Design

journal homepage: www.elsevier.com/locate/matdes

The effect of high strain rate impact in Yttria stabilized zirconia

Irati Sanchez [a], Dragos Axinte [a,*], Zhirong Liao [a,*], Oriol Gavalda-Diaz [a,b], Rob Smith [c]

[a] Rolls-Royce University Technology Centre (UTC) in Manufacturing and On-Wing Technology, Faculty of Engineering, University of Nottingham, UK
[b] Composites Research Group, Faculty of Engineering, University of Nottingham, NG7 2RD, UK
[c] Rolls-Royce plc, Derby, UK

HIGHLIGHTS

- When impacting 8YSZ at a small scale a martensitic transformation is triggered at high-strain rates but not at low.
- This martensitic transformation, proven by a Raman Spectroscopy, happens at a very surface (~600 nm) and at a localized manner.
- TEM analysis in high-strain rate impact areas confirm the presence of needle shape discontinuities that could become crack induction points.
- The result comparison between high and low strain rate impacts suggest a threshold rate inducing a martensitic transformation in 8YSZ.

GRAPHICAL ABSTRACT

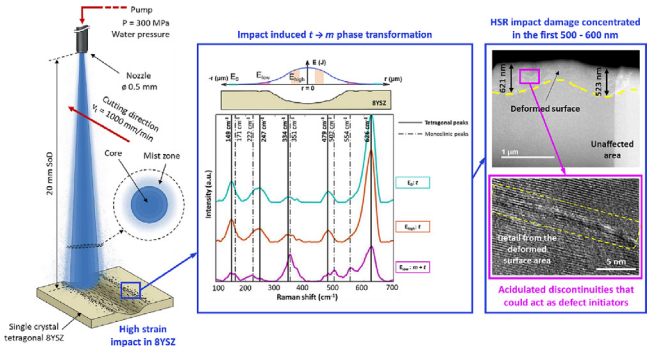

ARTICLE INFO

Article history:
Received 15 December 2022
Revised 1 April 2023
Accepted 3 April 2023
Available online 6 April 2023

Keywords:
Phase transformation
Strain rate sensitivity
Raman spectroscopy
Lattice defects
Yttria Stabilized Zirconia

ABSTRACT

Yttria stabilized zirconia (6-8YSZ) is widely used as a top coat in Thermal Barrier Coatings (TBCs) to protect metallic substrates. These coatings are exposed to severe high strain rate fields along their life, for example during the impact of debris happening in service or during coating removal in repair processes. In this work a water jet and a high strain rate nanoindenter are used to understand the effect of the strain rate (from 10^{-3} to 10^{8} s^{-1}) on the behaviour of 8YSZ at a small scale. It is observed how, at extremely high strain rates (10^{6}–10^{8} s^{-1}), the material suffers from a brittle-dominated failure which induces localized phase transformation. At lower strain rates (10^{-3}–1 s^{-1}), plasticity dominates, and phase transformation is not observed.

1. Introduction

Zirconia is a remarkable material for high temperature or harsh environment applications. This is due to its high melting point (2680 °C), low thermal conductivity and high resistance to chemical attacks. There are three polymorphic modifications of zirconia oxide (ZrO_2): monoclinic (*m*), tetragonal (*t*) and cubic (*c*). The usual transformation of these phases goes from monoclinic at room temperature and atmospheric pressure, to tetragonal by martensitic transformation (T_m) at 1170 °C and to cubic at 2370 °C until its melting point at 2690 °C [1 2].

The polymorphic transformation of ZrO_2 from tetragonal to monoclinic, when cooling below.

~ 950 °C, comes with a volume change of ~ 4% due to a diffusionless martensitic transformation to accommodate the Zr ions from an 8 to 7 fold coordination system [3,4]. When cooling, this

* Corresponding authors.
E-mail addresses: Dragos.Axinte@Nottingham.ac.uk (D. Axinte), Zhirong.Liao@-Nottingham.ac.uk (Z. Liao).

https://doi.org/10.1016/j.matdes.2023.111908
0264-1275/

creates a strain of ~ 1.5%, that occurs below the ductile to brittle transformation temperature [5], which leads to cracking, and consequently, to premature failure of the material [6,7].

On the other hand, when the zirconia undergoes the $t \rightarrow m$ martensitic transformation, the volume change generates compressive stresses. If this transformation is done in a controlled manner, the effect can be used as transformation toughening [8]. If the material has undergone transformation toughening, and cracks are generated under mechanical load, the compressive forces will close them, preventing their propagation and avoiding material failure. Due to this phenomena a material with high toughness, that is capable of dissipating energy under stress, and with a high fracture resistance is created [9].

One way of controlling the behaviour of Zirconia to achieve the required properties for each application is to add small quantities of oxides (e.g. Y_2O_3, CaO, MgO) [10] to partially or fully stabilize it [11]. Yttria (Y_2O_3) is one of the most effective stabilizers to avoid the transformation to a monoclinic (m) state [7] which enables the high temperature tetragonal (t) or cubic (c) phases to be stable at room temperature [12]. In the process, Zr^{4+} ions are randomly replaced by Y^{3+} ions which are slightly larger (i.e. 0.96 Å Y^{3+} and 0.84 Å Zr^{4+}) while the trivalent Y^{3+} ions induces O^{2-} oxygen vacancies in the ZrO_2 structure that is built up by Zr^{4+} tetravalent ions. The introduction of oxygen vacancies reduces the fold coordination number of the zirconia from 8 to < 8 at high temperature, hence preventing it from undergoing a $t \rightarrow m$ transformation when cooling down [4].

Adding different percentages of yttria produces materials with distinct properties, making them appropriate for specific applications. Yttria Stabilized Zirconia (YSZ) with a 6–8 wt% of Y_2O_3 is widely used as a top layer in Thermal Barrier Coatings (TBCs) to enhance the performance of metallic components of jet engines at temperatures well above their melting point [13,14]. 8 wt% of Yttria is considered a metastable phase with a tetragonal structure [15]. It would take 9 wt% Yttria to be fully stabilized, whose crystallographic structure is normally presented as cubic [2]. Having the right proportion of Y_2O_3 is key to achieve the high thermal expansion coefficient, good thermal shock resistance and good chemical stability required for TBCs. Increasing the amount of Y_2O_3 to obtain a fully stabilized YSZ would help with the thermal stability but would make the material more brittle and prone to cracking under mechanical stress [16]. With 8YSZ a good balance of material properties is achieved, but its fracture toughness tends to be on the lower side, approaching values similar to the monoclinic phase, which results in a limited amount of expected transformation toughening [2].

2. Theoretical background

Despite the numerous studies conducted on YSZ regarding its properties at high temperatures or in harsh environments, there is limited information on how mechanical loads affect its failure mechanisms. These mechanical loads can be easily originated either during in-service (e.g. impact by high-velocity small debris) or during processing (e.g. Water Jet machining) both in the range of high strain rate (HSR) impact. In this work, a Plain Water Jet (PWJ) was used to investigate the effect of mechanical loads, at a small scale, on the properties of YSZ which has relevance not only to manufacturing methods but also in-service like conditions of the surfaces coated with YSZ [17].

In Water Jet, the plume can be divided into three sections characterized by different water densities that decrease while the jet loses its focus: *continuous*, *open* and *diffused* jet regions as depicted in Fig. 1a and b. The PWJ milling process of the coating is performed at the *open* jet section mainly by the main core (that presents a high density and kinetic energy of the water droplets) while in the mist zone of this section (characterized by a lower density/kinetic energy than the main core) only secondary material removal occurs [18].

The aim of this paper is to investigate how 8YSZ behaves at small scale when being exposed to impacts at high and low strain rates. The tests will be conducted by using a PWJ and a controlled nanoindenter respectively, and subsequently the influence of the mechanical response of the material will be analysed. As such, this paper reports how in 8YSZ $t \rightarrow m$ transformations only happen at high strain rate (HSR) (>10^6 s^{-1}) but not low strain rate LSR (<1 s^{-1}).

3. Experimental procedure: Methodology and materials

For the present study a straight trench has been milled with a Plain Water Jet machine (i.e. without abrasives) as described in Fig. 1. A 0.5 mm orifice needle nozzle at a pressure of 300 MPa, 1000 mm/min feed rate and 20 mm stand of distance (SoD) that impacts the surface at HSR (calculated to be above 10^6 s^{-1} [19]) was used in a 10 mm × 10 mm × 2 mm single crystal 8YSZ sample. At these conditions the jet plume generates an impact on the target surface causing a strain rate of 10^6 to 10^8 s^{-1} [20]. Considering that the energy (E) released by the PWJ follows a Gaussian distribution along the width of the jet [21], the analysis areas have been selected as illustrated in Fig. 2 and are shown by using a Scanning Electron Microscope (SEM) (JEOL 7000F FEG-SEM):

i) E_0: control region where no jet energy has interacted with the sample (Fig. 2a). This area was analysed as reference material.
ii) E_{low}: area whereby the sample has been impinged by low water density mist zone of the jet and hence single droplet impacts can be identified; this is defined as low energy impact region (Fig. 2b).
iii) E_{high}: region whereby the surface has been milled by the high density droplets of the main core of the plume and as a result a trench is generated; the main core is the jet region that contains most of the jet's energy (Fig. 2c).

4. Results

4.1. High strain rate (HSR) impact study in YSZ

Raman spectroscopy is a well stablished technique in the study of phase transformation of YSZ [22]. Consequently, a Horiba LabRAM HR confocal Raman spectroscopy microscope (x50 lens; 0.55 numerical aperture) with λ 532 nm wavelength (i.e., green) laser, operating at a power of ~ 2 mW (100%) and a spot size of approximately 1.2 μm (calculated based on the Rayleigh criterion), has been used for identifying a $t \rightarrow m$ transformation in the three regions of the sample due to the impact energy of the PWJ.

Fig. 3 presents an example of many (>30) Raman spectra from the three regions (E_0, E_{low}, E_{high}) of interest that received different levels of energy from the jet. In it the peaks related to tetragonal (continuous line) and monoclinic (dotted line) phases can be identified. The raw data was then post processed by normalizing the intensity and applying a baseline correction based on the model developed by Schulze et al. [23] for a clearer identification of the peaks.

The Raman spectra of the measurements from E_0 (i.e. control/untouched region) shows prominent vibration modes at 149 cm^{-1}, 247 cm^{-1}, 344 cm^{-1}, 479 cm^{-1} and 626 cm^{-1}. The 149 cm^{-1}, 247 cm^{-1}, 344 cm^{-1} and 479 cm^{-1} vibration modes match with the literature values of typical t bands of 8YSZ [6-8,18,19]. However, the 626 cm^{-1} peak broadening, to the left side,

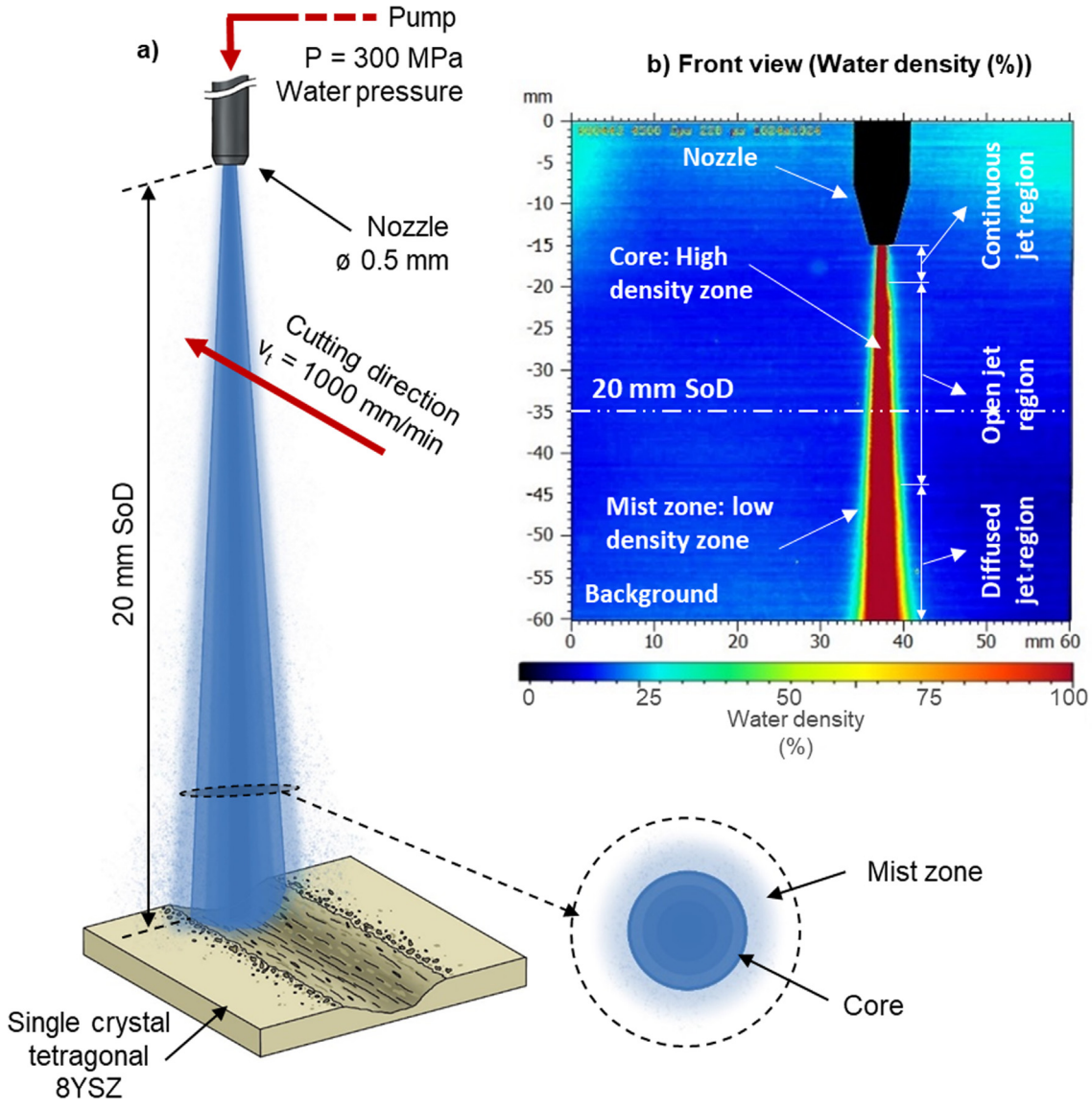

Fig. 1. a) Schematic representation of a PWJ trench indicating the process parameters in the performed tests b) Waterjet density distribution along the jet – experimental results.

suggests that this was created by the merge of two peaks: the 612 cm^{-1} and 640 cm^{-1} peaks reported in the literature as related to YSZ tetragonal phase [18]. Furthermore, the Raman spectra obtained from E_{high} present the same vibrational modes as the E_0 regions where no monoclinic *(m)* bands are observed, confirming the state of the material as fully tetragonal *(t)*. However, the Raman spectra measured in the E_{low} region, where single droplet impact occurs, shows two major changes: *i)* the appearance of two new peaks (i.e. 502 cm^{-1}, 554 cm^{-1}) that are related to $t \rightarrow m$ transformation, *ii)* and a clear variation in the vibration modes (i.e. ~ 200 cm^{-1} and 500 – 550 cm^{-1} domain) that are characteristic to *m* YSZ, as well as an increase in the intensity of the vibration mode at ~ 350 cm^{-1}. Both changes in the Raman spectra are indicators of a partial $t \rightarrow m$ diffusionless phase transformation after a single high strain impact caused, in our case, by high velocity droplet impact (HSR) at room temperature. This interesting phenomenon reveals the materials modification mechanism of 8YSZ under high strain rate mechanical impact.

Moreover, considering that a confocal Raman spectrometer just penetrates a relatively low depth into the examined material, it implies that the monoclinic 8YSZ has been transformed at the very surface in a much localized manner. In contrast, in the sample zone characterized by E_{high}, $t \rightarrow m$ phase change has not been registered; note that in this zone the high energy of the jet creates cracks on the material inducing a brittle fracture and removing the upper regions. Hence, due to the occurrence of material removal, in this region, new material is continuously exposed to the PWJ, situation that leads to "loss of history" of possible $t \rightarrow m$ transformations. Due to this the E_{low} area was used to understand the high strain rate microscale deformation and fracture.

Nonetheless, to reveal how the martensitic $t \rightarrow m$ transformation is happening at a nanoscale level in the E_{low} region, lamellas were extracted and prepared from a single droplet impacted 8YSZ surface using a Focused Ion Beam (FEI Quanta200 3D FIB-SEM). As shown in Fig. 3, Transmission Electron Microscopy (TEM) analysis has been further conducted to reveal how the shock affected the local microstructure.

Fig. 4a shows a TEM study of an E_{low} region. It can be observed that the damage induced by a high strain impact is concentrated within the first 500–600 nm. The diffraction contrast observed within that area suggested the formation of a highly deformed region. Fig. 4b shows high-resolution images of the defect present

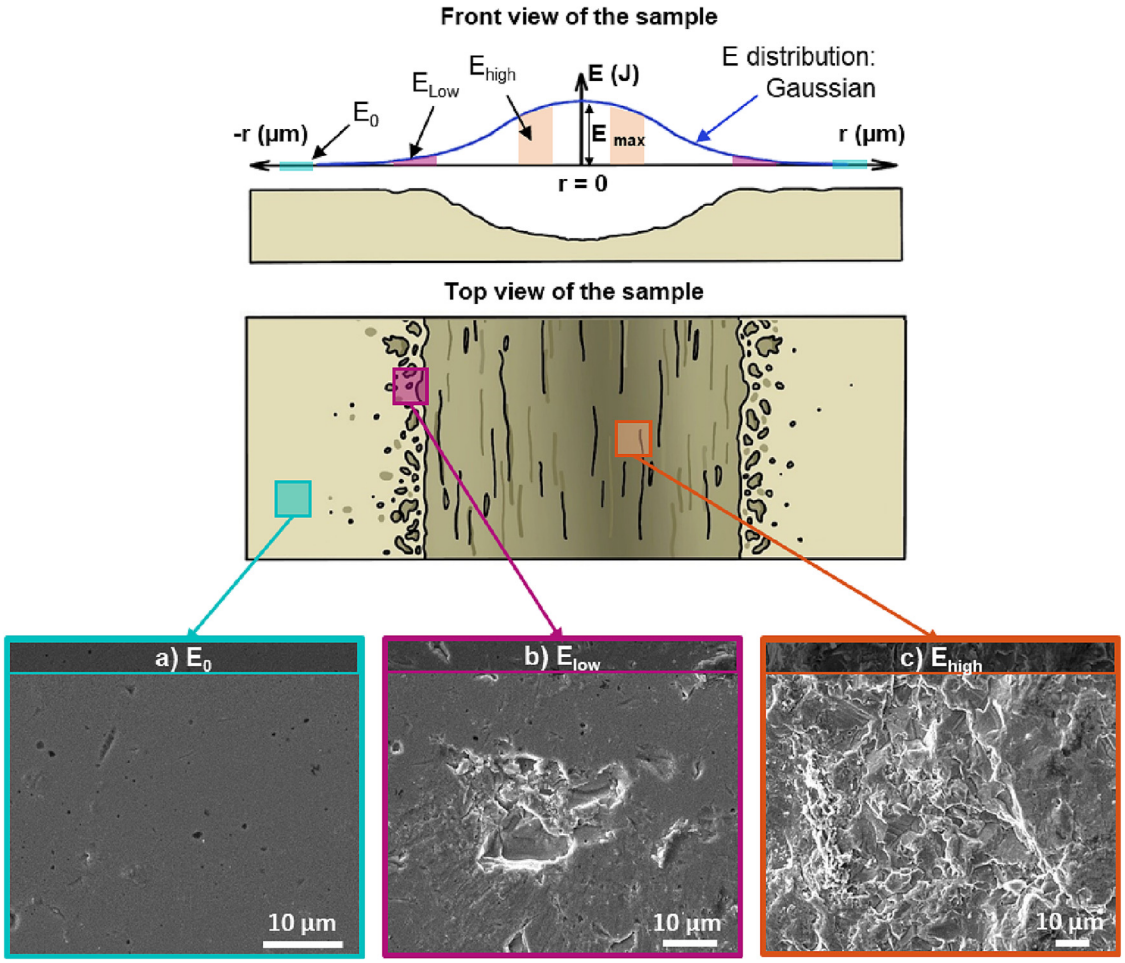

Fig. 2. Schematic representation of the front and top view of the PWJ milled trench indicating Gaussian energy distribution (E) of the jet and the location of the three regions of interest. Finally, SEM images of the selected surface areas: a) E_0, b) E_{low}, c) E_{high}, indicating the surface damage under mechanical impact.

in the deformed area. These show acidulated discontinuities at the atomic scale that could act as defect initiators (e.g. crack initiation zones). Fig. 4c shows another E_{low} region where cracks have propagated. Diffraction patterns from the surface inwards show the localised residual strain in the surface that gets relaxed in the bulk. It is believed that the propagation of cracks leads to a localised $t \rightarrow m$ transformation previously observed with Raman spectroscopy.

4.2. Low strain rate (LSR) impact analysis in YSZ

However, with the aim of observing the effect of the strain rate in 8YSZ nanoindentation tests have been performed in the region of 10^{-3} s^{-1} to 10 s^{-1}, which are considerably lower than the ones generated with the PWJ milling process that go over 10^6 s^{-1}. This situation offered the opportunity to explore the effect and differences that the strain rate can cause in the $t \rightarrow m$ transition phenomena by a single impact in a single crystal 8YSZ.

For this study, a SEM in-situ nanoindenter equipped with a diamond spherical tip (∅40 µm) was used to mimic the shape of the water droplet as much as possible and access lower values of strain rate. The indentations have been analysed by studying the relationship between the indentation depth (h) and the loading/unloading (P) forces that relate to the indentation energies and which are calculated from the area underneath the load and unload curve (Fig. 5a and b) [25]. Fig. 5c shows that the elastic/plastic ratio grows logarithmically while increasing the strain rate from 10^{-3} to 1 s^{-1} demonstrating a more brittle behaviour of the 8YSZ. Finally, Fig. 5d shows how the hardness is also strain rate dependent suggesting a strain hardening phenomena at room temperature generated by the creation of defects in the lattice structure, similar to the findings of D. Xiao et al. [26] in pure zirconia.

5. Discussion

The comparison of the SEM images of the low strain rate (LSR) indentations performed with the nanoindenter (Fig. 6a) with those obtained at high strain rate (E_{low} in Fig. 1e) support the analysis presented in Fig. 5c. While the craters generated at high strain (>10^6 s^{-1}) show evidence of brittle fracture, the indentations at low strain rates (10^{-3} to 1 s^{-1}) exhibit material pile up at the edge, indicating a more ductile behaviour. However, differences between the results obtained at the low range (i.e. 10^{-3} s^{-1} and 1 s^{-1}) can also be found, as cracking increases with the strain rate.

Moreover, it is also important to acknowledge that even if the setups of high and low strain rate have been compared to test the material properties, there are fundamental differences between them. PWJ droplets can be deformed and residual stresses redistributed when indenting the surface (at high strain) while for the diamond indentation the tip is considered non deformable [27]. However, this still demonstrates that a ductile to brittle transition at the micron scale can be achieved in 8YSZ when reaching high enough strain rates.

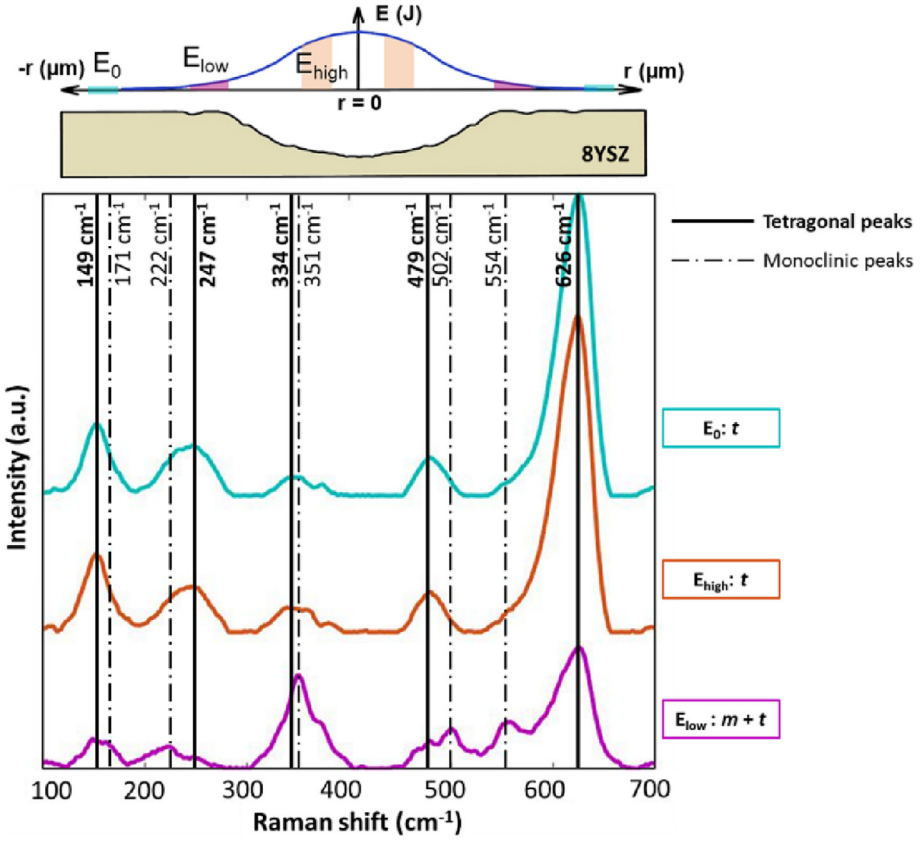

Fig. 3. Raman spectra from each of the three regions of interest: E_0, E_{low} and E_{high}. The analysis demonstrates $t \rightarrow m$ phase transformation phenomena in the zone of single droplet impact which is manifested by the appearance of new peaks (500–550 cm^{-1}), while in the trench, i.e. eroded, area and untouched surfaces show typical tetragonal spectra values.

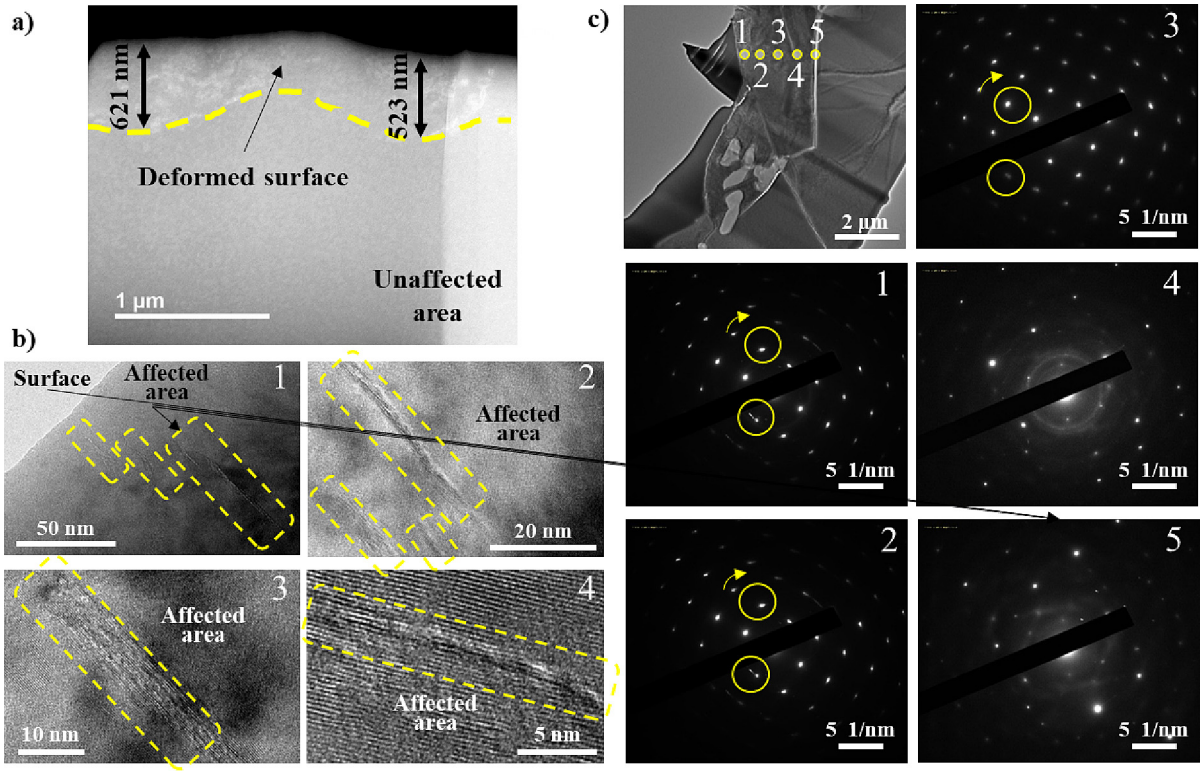

Fig. 4. A) general view of the lamella in the haadf stem in where defects created by the process can clearly be seen in the first 500 – 600 nm from the surface. b) BF TEM images showing an acicular dislocation build up that leads to the initial phases of a defect. c) SADP TEM diffraction patterns obtained from a STEM image of a HSR water droplet impact lamella (E_{low}) shows residual strain in the top being released while getting deeper beneath the surface while indicating a phase change when reaching the crack.

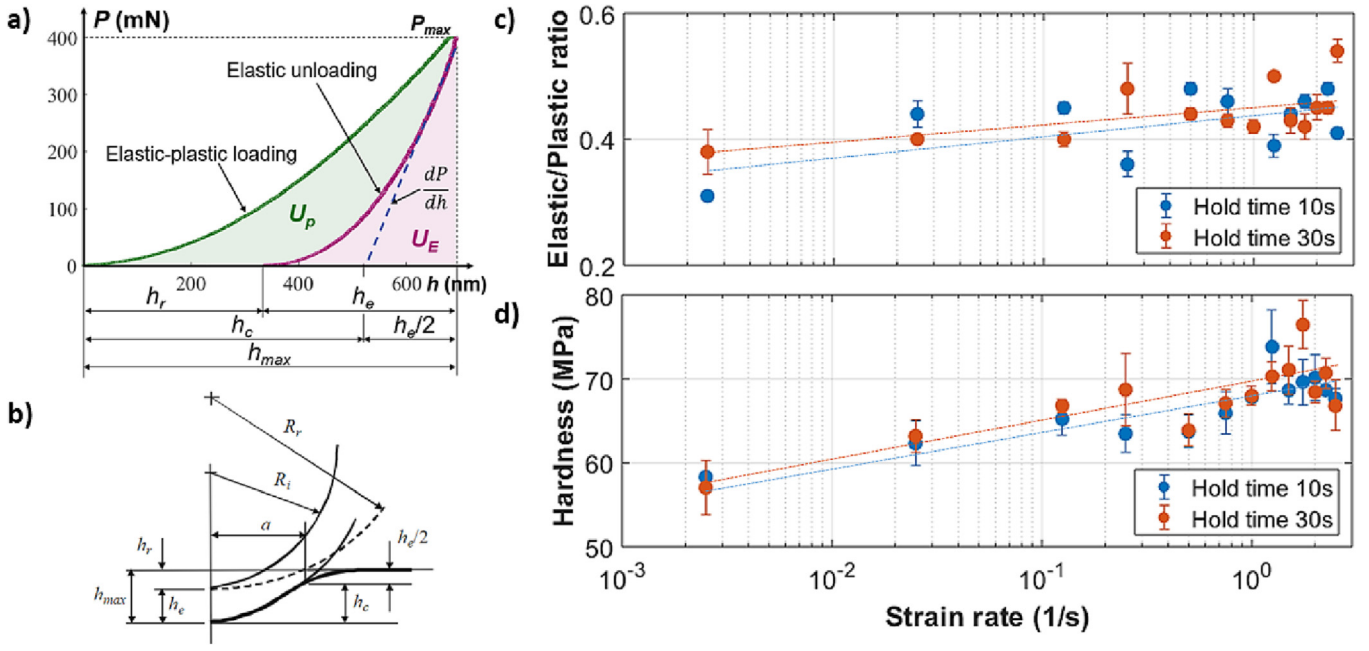

Fig. 5. A) exemplary *P-h* diagram obtained at 10 mN/s loading and 5 mN/s unloading and a 10 s hold time that describes the diagrams parameters and the schematic representation of the deformation under a spherical tip and b) the description of the relevant parameters (adapted from [24]). Comparison between c) Elastic /plastic ratio vs strain rate and d) Hardness vs strain rate; averaged results over 3 repeated measurements.

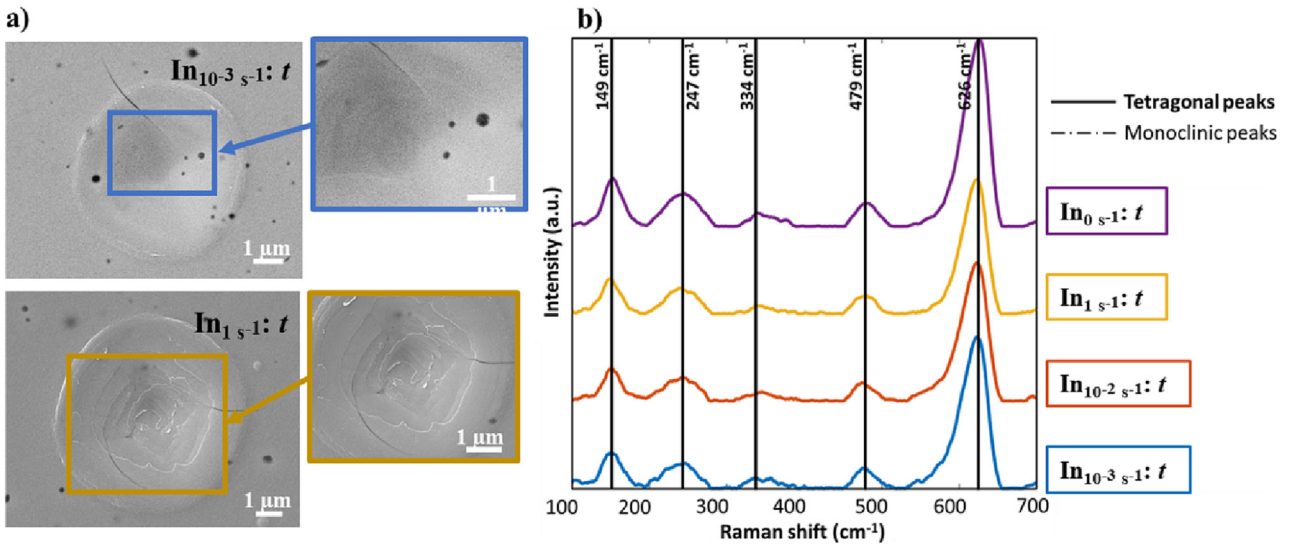

Fig. 6. A) SEM images of the indentations at 10^{-3} s^{-1} and 1 s^{-1} order of magnitude stain rates, b) Raman spectroscopy results of the indentation at all the analysed strain rates showing the absence of monoclinic phase.

In contrast with the high strain rate (HSR) results (>10^6 s^{-1} in Fig. 3) the Raman spectra for the LSR tests (from 10^{-3} to 1 s^{-1} in Fig. 6b) show that there is no $t \rightarrow m$ phase transformation. This suggests that the low strain rates are not enough to trigger this change (i.e. the elastic/plastic ration is too low) and hence that this transformation is linked to the speed required to propagate the discontinuities in zirconia or that at LSR not enough defects are generated to trigger any transformation.

With the results presented above, it can be concluded that the LSR deformation applied with a non-deformable tool induces a ductile deformation mechanism and no phase transformation. The fact that a phase transformation can be seen at HSR (>10^6 s^{-1}) whereas in the LSR indentations (10^{-3} to 1 s^{-1}) this is not observed, suggests that the phenomenon is strongly related to the strain rate and the ductile-to-brittle transition at the micron scale. That might also explain why this has not been previously reported. Furthermore, in order to fully identify what happens at different strain rates it would be interesting to, in future work, complete the range of strain rates missing in the presented results (i.e. from 1 s^{-1} to 10^6 s^{-1}).

6. Conclusions

Following the objective of investigating how 8YSZ behaves at small scale when being exposed to impacts at high and low strain

rates, it has been seen that 8YSZ $t \rightarrow m$ transformations only happen at high strain rates (>10^6 s^{-1}) but not at low (<1 s^{-1}). Hence, this arises the question if there is a threshold that could trigger this $t \rightarrow m$ transformation.

With the impact tests at HSR a $t \rightarrow m$ phase transformation has been reported after Raman spectroscopy analysis at the E_{low} region. This phenomenon happens in 8YSZ at the very surface and at a localized manner (in this case induced by PWJ impact). However, there is no transformation registered in the E_{high} zone as the high energy of the jet creates cracks on the material inducing a brittle fracture and removing the upper regions. Due to this occurrence of material removal, new material is continuously exposed to the PWJ, situation that leads to "loss of history" of possible $t \rightarrow m$ transformations.

Moreover, the high-resolution TEM analysis in high strain rate impact areas shows needle shape discontinuities oriented in a preferential direction. These affected the first ~ 600 nm from the surface, which could act as crack induction points. Multiple cracks have also been observed in those regions and it is believed that they could act as nucleation points for the phase transformation measured with Raman Spectroscopy.

On the other hand, micro indentations in 8YSZ, using a spherical indenter, at an interval of 10^{-3} s^{-1} to 1 s^{-1} strain rate shows that the elastic/plastic ratio and hardness grows logarithmically while increasing the strain rate. This demonstrates that the material behaving in a ductile or brittle manner is influenced by the strain rate.

Finally, for the indentations performed at the strain rates ranging between 10^{-3} s^{-1} and 1 s^{-1} there was no indication of $t \rightarrow m$ transformation. It is believed that this lack of phase transformation is linked to the absence of cracks dominating the failure mechanism.

Data availability

Data will be made available on request.

Declaration of Competing Interest

The authors declare that they have no known competing financial interests or personal relationships that could have appeared to influence the work reported in this paper.

Acknowledgments

The authors would like to thank Rolls-Royce plc. for the financial support and the provision of the material necessary for the development of the project. Also, big thanks to Stephen Hall, from the University of Nottingham, for his help in the set up and test performance of the Water Jet Machine tests. The authors are also grateful to the Nanoscale and Microscale Research Centre (nmRC) at the University of Nottingham for the support and the use of the facilities. This project got also support from Innovate UK through the Aerospace Technology Institute (ATI) under the project REINSTATE (51689) and EPSRC through the NanoPrime initiative (EPSRC Reference: EP/R025282/1).

References

[1] J.R. Kelly, I. Denry, Stabilized zirconia as a structural ceramic: An overview, Dent. Mater. 24 (2008) 289–298, https://doi.org/10.1016/j.dental.2007.05.005.
[2] J. Chevalier, L. Gremillard, A.V. Virkar, D.R. Clarke, The tetragonal-monoclinic transformation in zirconia: Lessons learned and future trends, J. Am. Ceram. Soc. 92 (2009) 1901–1920, https://doi.org/10.1111/j.1551-2916.2009.03278.x.
[3] R.H.J. Hannink, P.M. Kelly, B.C. Muddle, Transformation toughening in zirconia-containing ceramics, J. Am. Ceram. Soc. 83 (2000) 461–487, https://doi.org/10.1111/j.1151-2916.2000.tb01221.x.
[4] Y. Hemberger, C. Berthold, K.G. Nickel, Simultaneous phase and chemistry analysis in YSZ by Raman spectroscopy, 14th Bienn. Worldw. Congr. Unified Int. Tech. Conf. Refract. UNITECR 2015, Conjunction with 58th Int. Colloq. Refract., 2015.
[5] N.T. Paper, Overview of Zirconia With Respect to Gas Turhine Applications, 2019.
[6] V. Lughi, D.R. Clarke, High temperature aging of YSZ coatings and subsequent transformation at low temperature, Surf. Coatings Technol. 200 (2005) 1287–1291, https://doi.org/10.1016/j.surfcoat.2005.07.089.
[7] a.P. Naumenko, N.I. Berezovska, M.M. Biliy, O.V. Shevchenko, Vibrational analysis and Raman spectra of tetragonal Zirconia, Phys. Chem. Solid State. 9 (2008) 121–125.
[8] V. Kulyk, Z. Duriagina, A. Kostryzhev, B. Vasyliv, V. Vavrukh, O. Marenych, The Effect of Yttria Content on Microstructure, Strength, and Fracture Behavior of Yttria-Stabilized Zirconia, Materials (Basel). 15 (15) (2022) 5212.
[9] A. Loganathan, A.S. Gandhi, Effect of phase transformations on the fracture toughness of t' yttria stabilized zirconia, Mater. Sci. Eng. A. 556 (2012) 927–935, https://doi.org/10.1016/j.msea.2012.07.095.
[10] N.P. Padture, M. Gell, E.H. Jordan, Thermal Barrier Coatings for Gas-Turbine Engine Applications, Science 296 (5566) (2002) 280–284.
[11] A. Ghosh, A.K. Suri, M. Pandey, S. Thomas, T.R. Rama Mohan, B.T. Rao, Nanocrystalline zirconia-yttria system-a Raman study, Mater. Lett. 60 (2006) 1170–1173, https://doi.org/10.1016/j.matlet.2005.10.102.
[12] G.M. Wolten, Diffusionless Phase Transformations in Zirconia and Hafnia, J. Am. Ceram. Soc. 46 (1963) 418–422, https://doi.org/10.1111/j.1151-2916.1963.tb11768.x.
[13] D. Ushmaev, Z. Liao, A. Notron, D. Axinte, On the importance of interface stability in cellular automata models: Planar and dendritic solidification in laser melted YSZ, Mater. Des. 219 (2022), https://doi.org/10.1016/j.matdes.2022.110823 110823.
[14] A. Pakseresht, F. Sharifianjazi, A. Esmaeilkhanian, L. Bazli, M. Reisi Nafchi, M. Bazli, K. Kirubaharan, Failure mechanisms and structure tailoring of YSZ and new candidates for thermal barrier coatings: A systematic review, Mater. Des. 222 (2022) 111044.
[15] G. Bolelli, M.G. Righi, M.Z. Mughal, R. Moscatelli, O. Ligabue, N. Antolotti, M. Sebastiani, L. Lusvarghi, E. Bemporad, Damage progression in thermal barrier coating systems during thermal cycling: A nano-mechanical assessment, Mater. Des. 166 (2019) 107615.
[16] H. Masuda, K. Morita, M. Watanabe, T. Hara, H. Yoshida, T. Ohmura, Ferroelastic and plastic behaviors in pseudo-single crystal micropillars of nontransformable tetragonal zirconia, Acta Mater. 203 (2021), https://doi.org/10.1016/j.actamat.2020.11.013 116471.
[17] M.C. Kong, D. Axinte, W. Voice, Aspects of material removal mechanism in plain waterjet milling on gamma titanium aluminide, J. Mater. Process. Technol. 210 (2010) 573–584, https://doi.org/10.1016/j.jmatprotec.2009.11.009.
[18] Z. Liao, I. Sanchez, D. Xu, D. Axinte, G. Augustinavicius, A. Wretland, Dual-processing by abrasive waterjet machining—A method for machining and surface modification of nickel-based superalloy, J. Mater. Process. Technol. 285 (2020), https://doi.org/10.1016/j.jmatprotec.2020.116768 116768.
[19] W.F. Adler, Waterdrop impact modeling, Wear. 186–187 (1995) 341–351, https://doi.org/10.1016/0043-1648(95)07176-8.
[20] I.M. Hutchings, Strain rate effects in microparticle impact, J. Phys. D. Appl. Phys. 10 (14) (1977) L179–L184.
[21] I. Sanchez, D. Axinte, R. Smith, Modelling of rotational multiple plain water jets for controlled removal of multi-material coatings, CIRP Ann. 69 (1) (2020) 309–312.
[22] A. Portinha, V. Teixeira, J. Carneiro, M.G. Beghi, C.E. Bottani, N. Franco, R. Vassen, D. Stoever, A.D. Sequeira, Residual stresses and elastic modulus of thermal barrier coatings graded in porosity, Surf. Coatings Technol. 188–189 (2004) 120–128, https://doi.org/10.1016/j.surfcoat.2004.08.014.
[23] H.G. Schulze, R.B. Foist, K. Okuda, A. Ivanov, R.F.B. Turnera, A small-window moving average-based fully automated baseline estimation method for raman spectra, Appl. Spectrosc. 66 (2012) 757–764, https://doi.org/10.1366/11-06550.
[24] M.A. Peters, M. Apple, M. David, C. Kapitzke, S. Marginson, M. Olssen, F. Rizvi, S. Robertson, A. Tripathi, L.T. Smith, Nanoindentation, 2011. https://link-springer-com.libproxy.ucl.ac.uk/content/pdf/10.1007%2F978-94-6091-817-9.pdf.
[25] J. Ast, M. Ghidelli, K. Durst, M. Göken, M. Sebastiani, A.M. Korsunsky, A review of experimental approaches to fracture toughness evaluation at the micro-scale, Mater. Des. 173 (2019), https://doi.org/10.1016/j.matdes.2019.107762 107762.
[26] D. Xiao, Y. Li, S. Hu, L. Cai, High strain rate deformation behavior of zirconium at elevated temperatures, J. Mater. Sci. Technol. 26 (2010) 878–882, https://doi.org/10.1016/S1005-0302(10)60140-5.
[27] D. Axinte, H. Huang, J. Yan, Z. Liao, What micro-mechanical testing can reveal about machining processes, Int. J. Mach. Tools Manuf. 183 (2022), https://doi.org/10.1016/j.ijmachtools.2022.103964 103964.